Dark Count Rate Degradation in CMOS SPADs Exposed to X-Rays and Neutrons

Draft version July 5, 2018
Typeset using LaTeX default style in AASTeX62

Search for GeV Gamma-ray Counterparts of Gravitational Wave Events by *CALET*

O. Adriani,[1,2] Y. Akaike,[3,4] K. Asano,[5] Y. Asaoka,[6,7] M.G. Bagliesi,[8,9] E. Berti,[1,2] G. Bigongiari,[8,9] W.R. Binns,[10] S. Bonechi,[8,9] M. Bongi,[1,2] P. Brogi,[8,9] J.H. Buckley,[10] N. Cannady,[11] G. Castellini,[12] C. Checchia,[13,14] M.L. Cherry,[11] G. Collazuol,[13,14] V. Di Felice,[15,16] K. Ebisawa,[17] H. Fuke,[17] T.G. Guzik,[11] T. Hams,[3,18] M. Hareyama,[19] N. Hasebe,[6] K. Hibino,[20] M. Ichimura,[21] K. Ioka,[22] W. Ishizaki,[5] M.H. Israel,[10] K. Kasahara,[6] J. Kataoka,[6] R. Kataoka,[23] Y. Katayose,[24] C. Kato,[25] N. Kawanaka,[26,27] Y. Kawakubo,[28] H.S. Krawczynski,[10] J.F. Krizmanic,[18,3] K. Kohri,[29] T. Lomtadze,[9] P. Maestro,[8,9] P.S. Marrocchesi,[8,9] A.M. Messineo,[30,9] J.W. Mitchell,[4] S. Miyake,[31] A.A. Moiseev,[32,18] K. Mori,[6,17] M. Mori,[33] N. Mori,[2] H.M. Motz,[34] K. Munakata,[25] H. Murakami,[6] S. Nakahira,[35] J. Nishimura,[17] G.A. de Nolfo,[36] S. Okuno,[20] J.F. Ormes,[37] S. Ozawa,[6] L. Pacini,[1,12,2] F. Palma,[15,16] P. Papini,[2] A.V. Penacchioni,[8,38] B.F. Rauch,[10] S.B. Ricciarini,[12,2] K. Sakai,[18,3] T. Sakamoto,[28] M. Sasaki,[18,32] Y. Shimizu,[20] A. Shiomi,[39] R. Sparvoli,[15,16] P. Spillantini,[1] F. Stolzi,[8,9] J.E. Suh,[8,9] A. Sulaj,[8,9] I. Takahashi,[40] M. Takayanagi,[17] M. Takita,[5] T. Tamura,[20] N. Tateyama,[20] T. Terasawa,[35] H. Tomida,[17] S. Torii,[6,7,41] Y. Tsunesada,[42] Y. Uchihori,[43] S. Ueno,[17] E. Vannuccini,[2] J.P. Wefel,[11] K. Yamaoka,[44] S. Yanagita,[45] A. Yoshida,[28] and K. Yoshida[46]
(CALET Collaboration)

[1]*Department of Physics, University of Florence, Via Sansone, 1 - 50019 Sesto, Fiorentino, Italy*
[2]*INFN Sezione di Florence, Via Sansone, 1 - 50019 Sesto, Fiorentino, Italy*
[3]*Department of Physics, University of Maryland, Baltimore County, 1000 Hilltop Circle, Baltimore, MD 21250, USA*
[4]*Astroparticle Physics Laboratory, NASA/GSFC, Greenbelt, MD 20771, USA*
[5]*Institute for Cosmic Ray Research, The University of Tokyo, 5-1-5 Kashiwa-no-Ha, Kashiwa, Chiba 277-8582, Japan*
[6]*Research Institute for Science and Engineering, Waseda University, 3-4-1 Okubo, Shinjuku, Tokyo 169-8555, Japan*
[7]*JEM Utilization Center, Human Spaceflight Technology Directorate, Japan Aerospace Exploration Agency, 2-1-1 Sengen, Tsukuba, Ibaraki 305-8505, Japan*
[8]*Department of Physical Sciences, Earth and Environment, University of Siena, via Roma 56, 53100 Siena, Italy*
[9]*INFN Sezione di Pisa, Polo Fibonacci, Largo B. Pontecorvo, 3 - 56127 Pisa, Italy*
[10]*Department of Physics, Washington University, One Brookings Drive, St. Louis, MO 63130-4899, USA*
[11]*Department of Physics and Astronomy, Louisiana State University, 202 Nicholson Hall, Baton Rouge, LA 70803, USA*
[12]*Institute of Applied Physics (IFAC), National Research Council (CNR), Via Madonna del Piano, 10, 50019 Sesto, Fiorentino, Italy*
[13]*Department of Physics and Astronomy, University of Padova, Via Marzolo, 8, 35131 Padova, Italy*
[14]*INFN Sezione di Padova, Via Marzolo, 8, 35131 Padova, Italy*
[15]*University of Rome "Tor Vergata", Via della Ricerca Scientifica 1, 00133 Rome, Italy*
[16]*INFN Sezione di Rome "Tor Vergata", Via della Ricerca Scientifica 1, 00133 Rome, Italy*
[17]*Institute of Space and Astronautical Science, Japan Aerospace Exploration Agency, 3-1-1 Yoshinodai, Chuo, Sagamihara, Kanagawa 252-5210, Japan*
[18]*CRESST and Astroparticle Physics Laboratory NASA/GSFC, Greenbelt, MD 20771, USA*
[19]*St. Marianna University School of Medicine, 2-16-1, Sugao, Miyamae-ku, Kawasaki, Kanagawa 216-8511, Japan*
[20]*Kanagawa University, 3-27-1 Rokkakubashi, Kanagawa, Yokohama, Kanagawa 221-8686, Japan*
[21]*Faculty of Science and Technology, Graduate School of Science and Technology, Hirosaki University, 3, Bunkyo, Hirosaki, Aomori 036-8561, Japan*
[22]*Yukawa Institute for Theoretical Physics, Kyoto University, Kitashirakawa Oiwakecho, Sakyo, Kyoto 606-8502, Japan*
[23]*National Institute of Polar Research, 10-3, Midori-cho, Tachikawa, Tokyo 190-8518, Japan*
[24]*Faculty of Engineering, Division of Intelligent Systems Engineering, Yokohama National University, 79-5 Tokiwadai, Hodogaya, Yokohama 240-8501, Japan*
[25]*Faculty of Science, Shinshu University, 3-1-1 Asahi, Matsumoto, Nagano 390-8621, Japan*
[26]*Hakubi Center, Kyoto University, Yoshida Honmachi, Sakyo-ku, Kyoto, 606-8501, Japan*
[27]*Department of Astronomy, Graduate School of Science, Kyoto University, Kitashirakawa Oiwake-cho, Sakyo-ku, Kyoto, 606-8502, Japan*
[28]*College of Science and Engineering, Department of Physics and Mathematics, Aoyama Gakuin University, 5-10-1 Fuchinobe, Chuo, Sagamihara, Kanagawa 252-5258, Japan*
[29]*Institute of Particle and Nuclear Studies, High Energy Accelerator Research Organization, 1-1 Oho, Tsukuba, Ibaraki, 305-0801, Japan*
[30]*University of Pisa, Polo Fibonacci, Largo B. Pontecorvo, 3 - 56127 Pisa, Italy*
[31]*Department of Electrical and Electronic Systems Engineering, National Institute of Technology, Ibaraki College, 866 Nakane, Hitachinaka, Ibaraki 312-8508 Japan*
[32]*Department of Astronomy, University of Maryland, College Park, Maryland 20742, USA*
[33]*Department of Physical Sciences, College of Science and Engineering, Ritsumeikan University, Shiga 525-8577, Japan*
[34]*International Center for Science and Engineering Programs, Waseda University, 3-4-1 Okubo, Shinjuku, Tokyo 169-8555, Japan*

Corresponding author: Masaki Mori and Yoichi Asaoka
morim@fc.ritsumei.ac.jp; yoichi.asaoka@aoni.waseda.jp

[35]RIKEN, 2-1 Hirosawa, Wako, Saitama 351-0198, Japan
[36]Heliospheric Physics Laboratory, NASA/GSFC, Greenbelt, MD 20771, USA
[37]Department of Physics and Astronomy, University of Denver, Physics Building, Room 211, 2112 East Wesley Ave., Denver, CO 80208-6900, USA
[38]ASI Science Data Center (ASDC), Via del Politecnico snc, 00133 Rome, Italy
[39]College of Industrial Technology, Nihon University, 1-2-1 Izumi, Narashino, Chiba 275-8575, Japan
[40]Kavli Institute for the Physics and Mathematics of the Universe, The University of Tokyo, 5-1-5 Kashiwanoha, Kashiwa, 277-8583, Japan
[41]School of Advanced Science and Engineering, Waseda University, 3-4-1 Okubo, Shinjuku, Tokyo 169-8555, Japan
[42]Division of Mathematics and Physics, Graduate School of Science, Osaka City University, 3-3-138 Sugimoto, Sumiyoshi, Osaka 558-8585, Japan
[43]National Institutes for Quantum and Radiation Science and Technology, 4-9-1 Anagawa, Inage, Chiba 263-8555, JAPAN
[44]Nagoya University, Furo, Chikusa, Nagoya 464-8601, Japan
[45]College of Science, Ibaraki University, 2-1-1 Bunkyo, Mito, Ibaraki 310-8512, Japan
[46]Department of Electronic Information Systems, Shibaura Institute of Technology, 307 Fukasaku, Minuma, Saitama 337-8570, Japan

ABSTRACT

We present results on searches for gamma-ray counterparts of the LIGO/Virgo gravitational-wave events using CALorimetric Electron Telescope (*CALET*) observations. The main instrument of *CALET*, CALorimeter (CAL), observes gamma-rays from $\sim$ 1 GeV up to 10 TeV with a field of view of nearly 2 sr. In addition, the *CALET* gamma-ray burst monitor (CGBM) views $\sim$3 sr and $\sim 2\pi$ sr of the sky in the 7 keV – 1 MeV and the 40 keV – 20 MeV bands, respectively, by using two different crystal scintillators. The *CALET* observations on the International Space Station started in October 2015, and here we report analyses of events associated with the following gravitational wave events: GW151226, GW170104, GW170608, GW170814 and GW170817. Although only upper limits on gamma-ray emission are obtained, they correspond to a luminosity of $10^{49} \sim 10^{53}$ erg s^{-1} in the GeV energy band depending on the distance and the assumed time duration of each event, which is approximately the order of luminosity of typical short gamma-ray bursts. This implies there will be a favorable opportunity to detect high-energy gamma-ray emission in further observations if additional gravitational wave events with favorable geometry will occur within our field-of-view. We also show the sensitivity of *CALET* for gamma-ray transient events which is the order of 10^{-7} erg cm^{-2} s^{-1} for an observation of 100 s duration.

1. INTRODUCTION

The discovery of gravitational-wave (GW) events using laser interferometers by the LIGO and Virgo Scientific Collaborations (Abbott et al. 2016a) was an epoch-making development following the prediction of the existence of gravitational waves by Einstein (1916,1918) a hundred years earlier. GW events are thought to be produced in the last stage of merging compact binaries, and electromagnetic counterparts of these events have been extensively discussed by many authors. Merging neutron star – neutron star (NS-NS) binaries and neutron star – black hole (NS-BH) binaries are thought to emit significant amount of electromagnetic radiation (e.g. Phinney (2009); Rosswog (2015); Fernández and Metzger (2016)), while it is often assumed that gravitational-wave events resulting from the merger of stellar-mass black holes are unlikely to produce electromagnetic counterparts (e.g., De Mink and King (2017)).

Since the study of GW events is in the early stages, it is needless to say that the multimessenger approach is exceedingly important in order to understand the nature of the production mechanisms. Especially, mergers of NS-NS binaries are hypothesized to be a possible origin of short gamma-ray bursts (sGRBs) (e.g. Pacynski (1986); Goodman (1986); Eichler et al (1989); Narayan et al. (1992); Mochkovitch et al. (1993)) and thus the observation in the gamma-ray energy region is essential to understand the connection between sGRBs to GW events.

We summarize the characteristics of six GW events during the first and second advanced LIGO-Virgo observing runs in Table 1 with inferred parameters. We then report the analysis of *CALET*/CAL observations corresponding to these gravitational events (except GW150914, which occurred before the start of *CALET* operations) in the gamma-ray energy region as briefly summarized in Table 1.

Table 1. Summary of CALET observations of gravitational events reported by the Virgo and LIGO scientific collaborations (BH: black hole, NS: neutron star) and representative results from CALET observation (see text for other time windows.)

GW event	Time T_0 (UTC)	Location area (deg^2)	Luminosity distance (Mpc)	Event Type	Ref.	CALET resullts [time window]			
						Mode	Summed LIGO probability	Upper limits (90% C.L.) Energy flux ($erg\,cm^{-2}s^{-1}$)	Luminosity ($erg\,s^{-1}$)
GW150914	2015-09-14 09:50:45	600	440^{+160}_{-180}	BH-BH	[a]			Before operation	
GW151226	2015-12-26 09:54:43	850	440^{+180}_{-190}	BH-BH	[b]	LE	15%	$[T_0 - 525s, T_0 + 211s]$ 9.3×10^{-8}	2.3×10^{48}
GW170104	2017-01-04 10:11:58	1200	880^{+450}_{-390}	BH-BH	[c]	HE	30%	$[T_0 - 60s, T_0 + 60s]$ 6.4×10^{-6}	6.2×10^{50}
GW170608	2017-06-08 02:01:16	520	340^{+140}_{-140}	BH-BH	[d]	HE		$[T_0 - 60s, T_0 + 60s]$ Out of FOV	
GW170814	2017-08-14 10:30:43	60	540^{+130}_{-210}	BH-BH	[e]	HE		$[T_0 - 60s, T_0 + 60s]$ Out of FOV	
GW170817	2017-08-17 12:41:04	28	40^{+8}_{-14}	NS-NS	[f]	HE		$[T_0 - 60s, T_0 + 60s]$ Out of FOV	

Ref. [a] Abbott et al. (2016c), [b] Abbott et al. (2016b), [c] Abbott et al. (2017a), [d] Abbott et al. (2017f), [e] Abbott et al. (2017b), [f] Abbott et al. (2017c),

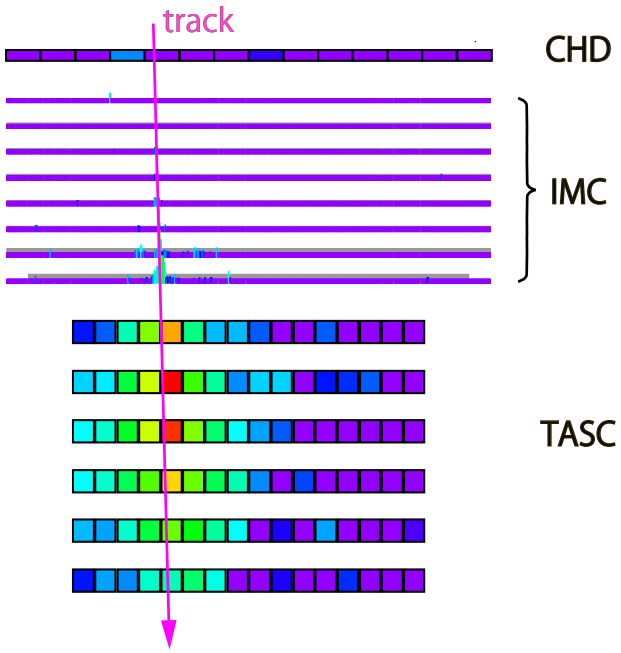

Figure 1. Schematic cross-sectional view of *CALET*/CAL with a sample event. We require that a track should cross the CHD (full area) and have at least a minimum path length in the TASC (see Cannady et al. (2017, 2018) for details).

2. OBSERVATION AND ANALYSIS

2.1. *CALET observation*

The CALorimetric Electron Telescope (*CALET*) mission (Torii et al. 2015) was launched and placed on the Japanese Experiment Module-Exposed Facility of the International Space Station (ISS) in 2015 August. At the LIGO trigger time of GW150914, *CALET* was in its commissioning phase and no observational data were available. It was fully **functional** at the trigger times of GW151226, GW170104, GW170608, GW170814, and GW170817.

There are two scientific instruments onboard *CALET*: (1) The Calorimeter (CAL), the main instrument, is a 30 radiation length deep calorimeter which can observe high-energy lectrons in the energy range ~ 1 GeV – ~ 20 TeV, protons, helium, and heavy nuclei in the energy range ~ 10 GeV – ~ 1000 TeV and gamma-rays in the energy range ~ 1 GeV – ~ 10 TeV. The field of view (FOV) of CAL extends to ~ 45° from the zenith direction. For gamma rays, the energy resolution and the angular resolution are estimated as 3% and 0.4°, respectively, at 10 GeV (Mori et al. 2013; Cannady et al. 2017, 2018). CAL consists of three main components: the CHarge Detector (CHD), the IMaging Calorimeter (IMC), and the Total AbSorption Calorimeter (TASC) (Figure 1). CHD is made up of a set of X and Y-direction arrays of 14 plastic scintillator paddles (32 mm × 10 mm × 450 mm); IMC is composed of 8 layers of X- and Y-direction arrays of 448 scintillation fibers (SciFi, 1 mm × 1 mm × 448 mm) separated by tungsten plates with a total thickness of 3 radiation lengths (X_0); and TASC is made of 6 layers of X- and Y-arrays of 16 lead tungstate ($PbWO_4$ or PWO) scintillation crystals (19 mm × 20 mm × 326 mm) with a total thickness of 27 X_0. (See Asaoka et al. (2017) for details.) The performance of CAL for gamma rays and initial results for steady gamma-ray sources are described in Cannady et al. (2017, 2018). (2) A companion instrument, the *CALET* Gamma-ray Burst Monitor (CGBM), monitors gamma-ray bursts (GRBs) using two different kinds of crystal scintillators ($LaBr_3$(Ce) and $Bi_4Ge_3O_{12}$ (BGO)) to cover a wide energy range (7 keV – 20 MeV) (Yamaoka et al. 2013). Results from CGBM are presented separately (Yamaoka et al. 2017).

We use two trigger modes of CAL for gamma-ray analysis: a low-energy gamma-ray (LE-γ) mode with an energy threshold ~ 1 GeV used at low geomagnetic latitudes and following a CGBM burst trigger, and a high-energy (HE) mode with a threshold ~ 10 GeV used in normal operation for all particles irrespective of geomagnetic latitude (Asaoka et al. 2018). Around the trigger time of GW151226, between 03:30 and 03:43 UT, CAL was collecting regular scientific data under the LE-γ mode. The high voltages supplied to photomultipliers of CGBM detectors were set at the nominal values around 03:22 UT and turned off around 03:43 UT to avoid a high background radiation area. No CGBM on-board trigger was generated at the trigger time of GW151226. For other GW events (GW170104, GW170608, GW170814 and GW170817), CAL was collecting data in the HE mode since the ISS was in the high latitude region in its orbit. First results on the analysis of GW151226 have already been published

(Adriani et al. 2016), and here we describe results with a refined analysis. We also give results on the comprehensive analysis of the CAL data for these four later events.

2.2. *Analysis of gamma-ray events in CALET/CAL*

The selection process of gamma-ray events used for the HE mode is essentially the same as described in Mori et al. (2013). For the LE-γ mode the selection and analysis are fully described in Cannady et al. (2017, 2018). Here we summarize the procedures briefly.

Offline trigger—In order to remove the effects of variation in the hardware trigger threshold and gains in the flight data sample, energy deposit thresholds higher than those nominally applied by the hardware trigger are imposed off-line both for LE-γ and HE modes.

Tracking—Event tracks are reconstructed for the HE mode using the EM track algorithm (Akaike et al. 2013) developed for the electron analysis which is a powerful method for reconstructing electromagnetic showers. For the LE-γ mode we use the CC track algorithm (Cannady et al. 2017, 2018) optimized for photons with energies below 10 GeV. It begins by finding clusters of hit fibers in the three bottom layers of IMC separately for the X and Y-projections and extending the candidate tracks to the upper layers of IMC. The trajectory with the highest total energy deposit is selected. In the HE mode, contained events passing through the CHD with track lengths in TASC in excess of 26.4 cm are subjected to further analysis; in LE-γ mode, in order to maximize the FOV, we select well contained events whose tracks satisfy more sophisticated geometrical conditions (Cannady et al. 2017, 2018).

Shower shape/hadronic rejection—Low energy gamma-ray events can be mimicked by albedo (i.e. upward moving) secondary charged pions from hadronic interactions in the calorimeter or the support structure. These events are vetoed by requiring that more energy be deposited in the bottom IMC layer than in the layer where pair conversion occurs. Further rejection of events with showers not consistent with a pure electromagnetic cascade is provided by a cut on the IMC concentration, which uses the lateral spread of the energy deposit distribution in the lower layers of IMC.

In order to reject hadronic events we utilize the K parameter defined as

$$K = \log_{10} F_E + R_E/2\,\mathrm{cm}$$

where F_E is the fractional energy deposit in the bottom TASC layer with respect to the total energy deposit sum in the TASC and R_E is the second moment of the lateral energy deposit distribution in the top layer of TASC. This method is developed for the derivation of the electron flux and is designed to exploit the larger spread and slower development of proton showers due to penetrating secondary pions (Adriani et al. 2017).

Zero charge identification—In order to select events consistent with zero primary charge, cuts are made on the energy deposits in CHD and upper IMC layers. These requirements are designed to veto charged particle events effectively. We require one of three filters utilizing CHD and upper IMC layers (see Cannady et al. (2017, 2018) for detail).

In addition, as described in detail in Cannady et al. (2017, 2018), we have to reject gamma-ray candidate events which are generated in the ISS structures such as the Japanese Experiment Module) to remove events generated in interactions of cosmic rays with these structures, which create gamma-ray event clusters clearly seen in our FOV. After these selections, incident gamma-ray energies are derived from the deposited energies based on Monte Carlo simulations, pre-flight accelerator calibrations, and in-flight non-interacting penetrating particle events.

Based on the CALET simulation studies (Mori et al. 2013; Cannady et al. 2017, 2018), the gamma-ray efficiency reaches its maximum around 10 GeV with an efficiency of 48% relative to an area of the TASC top layer (excluding a 1.9 cm margin around the outside) for normal incidence, after applying the event selections described above. This figure is to be compared with a pair creation probability of 54% in 1 radiation length, which is approximately the thickness required to be tracked in at least 3 layers in IMC, and implies a high efficiency in the gamma-ray event reconstruction and selection processes. The effective areas for four ranges of incident angles are shown in Figure 2 as a function of gamma-ray energy.

The GeV sky is rather bright along the Galactic plane due to the Galactic diffuse gamma-ray radiation with Galactic and extra-galactic individual sources, and there is a residual all-sky emission component called the isotropic diffuse gamma-ray background. These gamma-rays are a source of background in a search for gamma-ray emission associated with GW events. The expected number of background events in the time window used in our search was calculated using a prediction based on the Fermi LAT

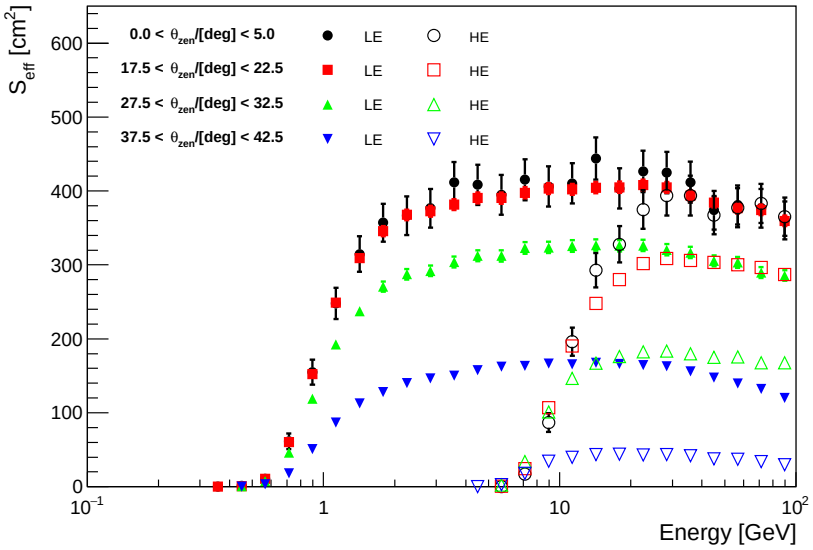

Figure 2. Effective area of *CALET*/CAL as a function of gamma-ray energy in the low-energy gamma-ray mode (LE-γ) and high-energy mode (HE). Four ranges of incident zenith angles (θ_{zen}) are assumed. Statistical uncertainties due to Monte Carlo statistics are shown by error bars.

Pass 8 measurements[1]. As shown by Cannady et al. (2017, 2018), the CALET measurement is in reasonable agreement with the LAT result.

The upper limit of the CAL observation in the time windows is estimated as follows: First, we calculate the effective area as a function of gamma-ray energy, and the resultant energy-dependent exposure map in the time window for the corresponding energy region depending on the trigger mode (LE-γ or HE). In the case of a null event, we estimate the upper limit on the gamma-ray flux corresponding to 2.44 events (the 90% confidence limit for a null observation) assuming a power-law spectrum with a single photon index of -2 by using the calculated exposure map. The photon index, -2, is taken as a typical value for *Fermi*-LAT GRBs in the GeV energy range (Ackermann et al. 2013).

2.3. *GW151226*[2]

We searched for gamma-ray events associated with GW151226 using the CAL data in the time window $[T_0 - 525\,\mathrm{s}, T_0 + 211\,\mathrm{s}]$ around the LIGO trigger time (T_0), the time period when the CAL was operational in the LE-γ mode with an energy threshold of 1 GeV. We analyzed the full length of this window in order to perform the most sensitive search possible with increased statistics.

Expected number of contaminated background gamma-rays is small because the searched area of the sky for the GW151226 counterpart is significantly apart from the Galactic plane. In fact, the number of expected background evens is 0.051 in this time window for the sky region covering 25% of the summed LIGO probabilities; i.e., the CAL observation is almost background-free for such a short time period. No candidates were found in this time window and sky region, resulting in an upper limit is calculated as described in the previous section.

Figure 3 shows the sky map of the 90%-confidence-level upper limit on the gamma-ray flux. The estimated upper limit is 9.3×10^{-8} erg cm^{-2} s^{-1} (90% C.L.) in the 1 – 10 GeV region where the coverage of CAL reaches 15% of the integrated LIGO probability ($\sim$ 1.1 sr). If we enlarge the sky region to contain 25% of the LIGO integrated probability, the upper limit is 2.8×10^{-7} erg cm^{-2} s^{-1} in the same energy region. The luminosity upper limit set by CAL is estimated as $2.3\,(6.8) \times 10^{48}$ erg s^{-1} assuming a luminosity distance of 440 Mpc for coverage of $\sim$ 15 (25)% of the LIGO integrated probability regions. By comparison, the upper limit in the energy flux in the 0.1 – 1 GeV region as reported by *Fermi*-LAT (assuming a power-law spectrum with a single photon index of -2) is 3×10^{-10} erg cm^{-2} s^{-1} (95% C.L.) for the time window $[T_0, T_0 + 1 \times 10^4\,\mathrm{s}]$ (Racusin et al. 2017), corresponding to $\sim 4 \times 10^{-9}$ erg cm^{-2} s^{-1} for the 736-s time window of the CAL in the LEγ mode for this GW event.

[1] We utilized a gamma-ray skymap in the energy range 1 – 100 GeV created using the archival data for the dates 2008-08-04 through 2017-03-12 available via https://fermi.gsfc.nasa.gov/ssc/data/access/lat/.

[2] The result shown here is an improved version based on more refined analysis compared with that presented in our previous paper (Adriani et al. 2016).

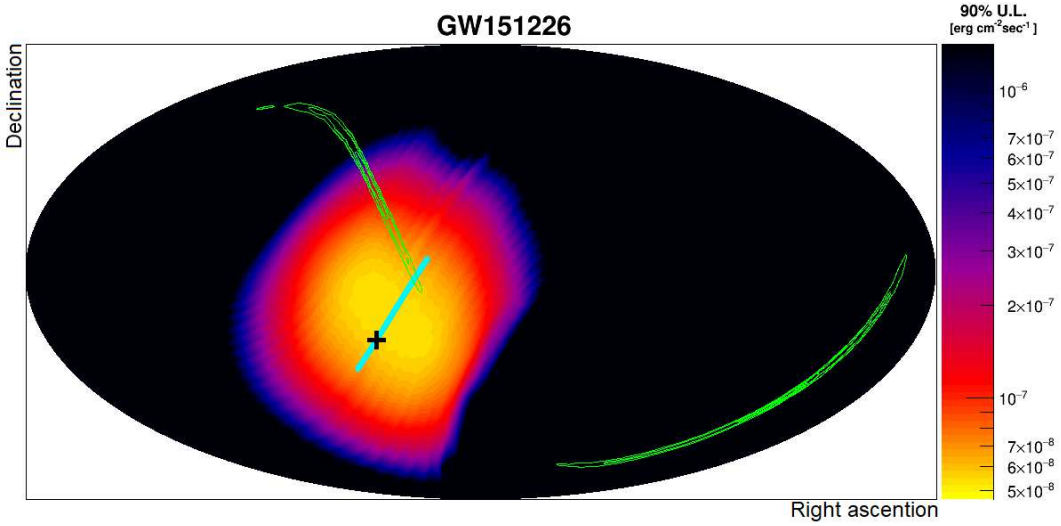

Figure 3. 90% C.L. upper limit on GW151226 energy flux in the energy region 1 – 10 GeV and time window $[T_0 - 525\,\mathrm{s}, T_0 + 211\,\mathrm{s}]$ shown in the equatorial coordinates. Thick cyan line shows the locus of the FOV center of CAL, and the plus symbol is that at T_0. Also shown by green contours is the localization significance map of the GW151226 signal reported by LIGO.

We also calculate upper limits on energy flux of gamma rays in smaller time windows since we do not know the time profile of the possible electromagnetic emission which accompanies gravitational wave events. When we set the window as $[T_0 - 60\,\mathrm{s}, T_0 + 60\,\mathrm{s}]$, the upper limit in the 1 – 10 GeV region is $9.4\,(20) \times 10^{-7}$ erg cm^{-2}s^{-1} for the integrated LIGO probabilities inside the CAL FOV of $\sim 15\,(25)\%$. If we set the window as $[T_0 - 1\,\mathrm{s}, T_0 + 1\,\mathrm{s}]$, the upper limit in the 1 – 10 GeV region is 5.3×10^{-5} erg cm^{-2} s^{-1} for the LIGO integrated probabilities in the CAL FOV at the level of $\sim 15\%$.

2.4. *GW170104*

For the time period around the trigger time (T_0) corresponding to GW170104, CAL was running in the HE mode with an energy threshold of 10 GeV. Gamma-ray events have been searched for using the CAL data in the time window $[T_0 - 60\,\mathrm{s}, T_0 + 60\,\mathrm{s}]$ but no candidates were found. The estimated number of background events expected in this time window is 7.8×10^{-4}. We calculated an upper limit on the gamma-ray energy flux of 6.4×10^{-6} erg cm^{-2} s^{-1} at 90% C.L. in the 10 – 100 GeV energy region for the sky region covering 30% of the integrated LIGO probabilities (Figure 4). This upper limit corresponds to 6.2×10^{50} erg s^{-1} assuming a luminosity distance of 880 Mpc. If we set a narrower time window as $[T_0 - 1, T_0 + 1\,\mathrm{s}]$, the estimated number of background events is 1.2×10^{-5} and the upper limit is 4.3×10^{-4} erg cm^{-2} s^{-1} for the flux and 4.1×10^{52} erg s^{-1} for the luminosity (90% C.L.) assuming the same sky region.

We note that *AGILE* reported a weak (4.4σ) event lasting about 32 ms and occurring 0.46 ± 0.05 s before T_0 in the omni-directional MCAL data in the 0.4 – 100 MeV region (Veracchia et al. 2017a), while other searches for high-energy emission yielded upper limits only.

2.5. *GW170608*

For the time period around the trigger time (T_0) corresponding to GW170608, CAL was running in the HE mode with an energy threshold of 10 GeV. Gamma-ray events have been searched for using the CAL data in the time window $[T_0 - 60\,\mathrm{s}, T_0 + 60\,\mathrm{s}]$ but no candidates were found. Unfortunately, the sky coverage of CAL did not include the region of the localization (520 deg^2) determined with two interferometric detectors as shown in Figure 5.

We note that *Fermi*-LAT reported a weak (3.5σ) excess around the LIGO location area in the $[T_0, T_0 + 1\,\mathrm{ks}]$ window in the energy region above 100 MeV (Omodei et al. 2017), but others reported only upper limits for high-energy emission for this GW event.

2.6. *GW170814*

For the time period around the trigger time (T_0) corresponding to GW170814, CAL was running in the HE mode with an energy threshold of 10 GeV. Gamma-ray events have been searched for using CAL data in the time window $[T_0 - 60\,\mathrm{s}, T_0 + 60\,\mathrm{s}]$

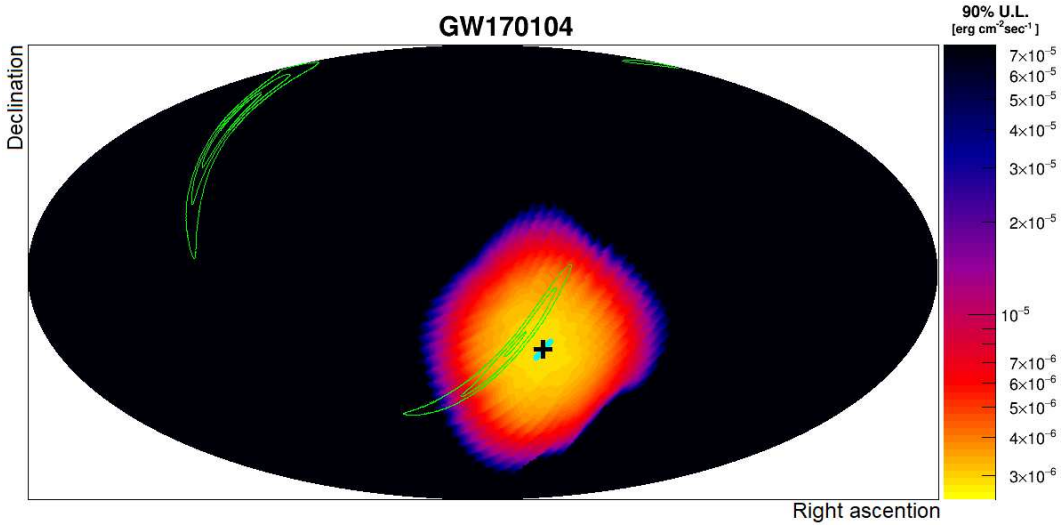

Figure 4. 90% C.L. upper limit on GW170104 energy flux in the energy region 10 – 100 GeV and time window $[T_0 - 60\ \mathrm{s}, T_0 + 60\ \mathrm{s}]$ shown in the equatorial coordinates. Thick cyan line shows the locus of the FOV center of CAL, and the plus symbol is that at T_0. Also shown by green contours is the localization significance map of the GW170104 signal reported by LIGO.

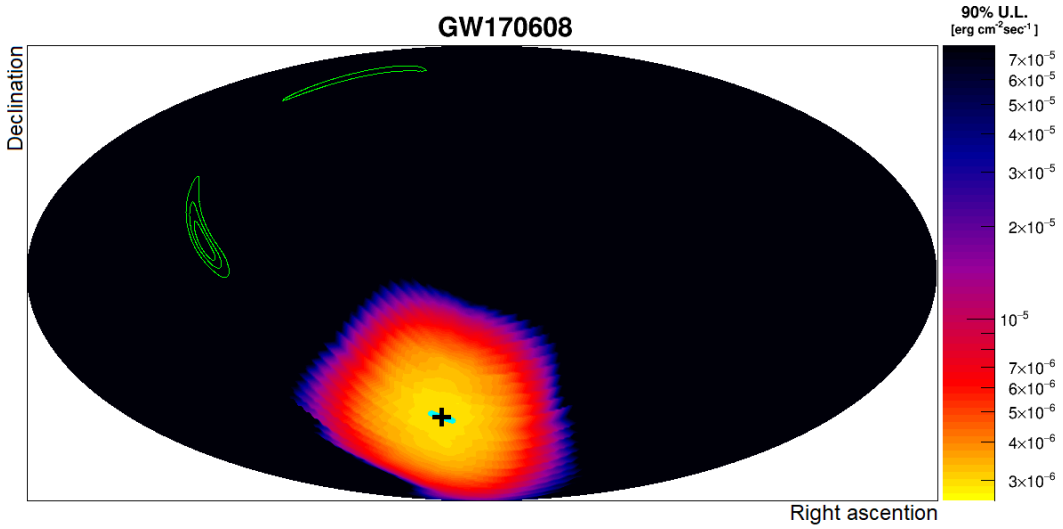

Figure 5. 90% C.L. upper limit on GW170608 energy flux in the energy region 10 – 100 GeV and time window $[T_0 - 60\ \mathrm{s}, T_0 + 60\ \mathrm{s}]$ shown in the equatorial coordinates. Thick cyan line shows the locus of the FOV center of CAL, and the plus symbol is that at T_0. Also shown by green contours is the localization significance map of the GW170608 signal reported by LIGO.

but no candidates were found. Unfortunately, the sky coverage of CAL did not include the rather small region of the localization (60 deg^2) determined with three interferometric detectors, as shown in Figure 6.

We note that *INTEGRAL*/SPI-ACS reported a weak 3.5σ excess in the $[T_0 - 1.5\ \mathrm{s}, T_0 + 8.5\ \mathrm{s}]$ window (Pozanenko et al. 2017), but this was not confirmed by an independent analysis (Savchenko et al. 2017). Other reports gave only upper limits on high-energy emission for this GW event.

2.7. *GW170817*

1.7 s after the trigger due to the LIGO-Virgo event GW170817 (T_0), *Fermi*-GBM and *INTEGRAL* detected GRB 170817A with T_{90} duration 2.0 ± 0.5 s (Abbott et al. 2017d). For the time period around GW 170817, CAL was running in the HE mode with an energy threshold of 10 GeV. Gamma-ray events have been searched for using the CAL data in the time window $[T_0 - 60\ \mathrm{s}, T_0 + 60\ \mathrm{s}]$ but no candidates were found. Unfortunately, the sky coverage of CAL did not include the rather small region

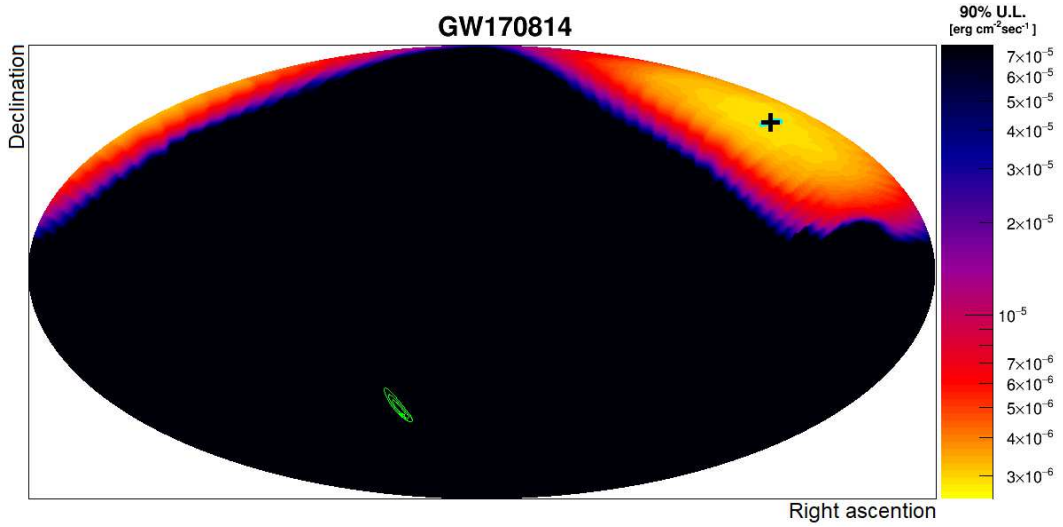

Figure 6. 90% C.L. upper limit on GW170814 energy flux in the energy region 10 – 100 GeV and time window $[T_0 - 60\ \mathrm{s}, T_0 + 60\ \mathrm{s}]$ shown in the equatorial coordinates. Thick cyan line shows the locus of the FOV center of CAL, and the plus symbol is that at T_0. Also shown by green contours is the localization significance map of the GW170814 signal reported by LIGO/Virgo.

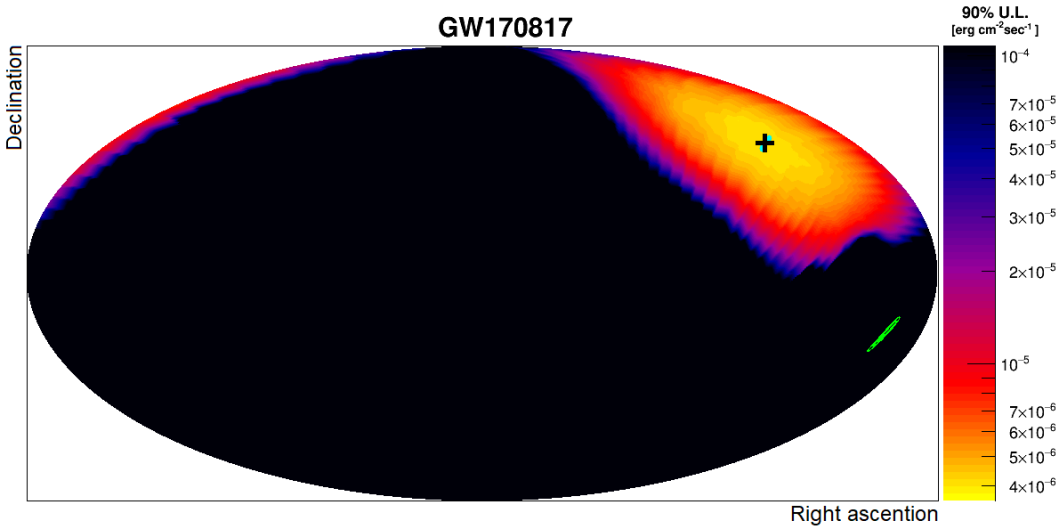

Figure 7. 90% C.L. upper limit on GW170817 energy flux in the energy region 10 – 100 GeV and time window $[T_0 - 60\ \mathrm{s}, T_0 + 60\ \mathrm{s}]$ shown in the equatorial coordinates. Thick cyan line shows the locus of the FOV center of CAL, and the plus symbol is that at T_0. Also shown by green contours is the localization significance map of the GW170817 signal reported by LIGO/Virgo.

of the localization (28 deg^2) determined with three interferometric detectors, as shown in Figure 7. It is reported the gravitational wave signal started about 100 s before T_0, but it was also out of the field-of-view of CAL during this period.

We have also searched for possible delayed signal from this merger event (Murase et al. 2018). In the two-month period (Aug. 17 – Oct. 16, 2017) after the event we had no gamma-ray candidate around the direction of its counterpart object (NGC 4993) (Abbott et al. 2017e), and obtained 90% C.L. upper limits on the energy flux of 1.2×10^{-10} erg cm^{-2}s^{-1} (4.0×10^{-10} erg cm^{-2}s^{-1}) for gamma rays above 1 GeV (10 GeV) using the LE-γ mode (the HE mode). This upper limit corresponds to 2.4×10^{43} erg s^{-1} (8.0×10^{43} erg s^{-1}) assuming a luminosity distance of 40 Mpc.

3. FUTURE PROSPECTS

Identifying the electromagnetic counterpart of a gravitational-wave event would be a key discovery to constrain the origin of the event. The detection of multiwavelength radiation in association with GW170817 (Abbott et al. 2017e) was a huge step to open a new window of astronomy. In particular the detection of a gamma-ray burst, GRB170817A, observed $\sim$ 1.7 s after GW170817 by *Fermi*-GBM and *INTEGRAL* (Abbott et al. 2017d), provides new insight into the origin of short gamma-ray bursts. The association of GW170817 and GRB170817A can be interpreted as a merger of a neutron star-neutron star binary, which is hypothesized to be a possible origin of short gamma-ray bursts as discussed in section 1. However, GRB170817A, which is the closest short GRB ever observed, is 2 to 6 orders of magnitude less energetic than other bursts with known distances.

The underluminous nature of GRB 170817A may imply that the gamma-rays detected with *Fermi*-GBM are off-axis emission from a typical short GRB (Abbott et al. 2017c; Alexander et al. 2018; Ioka & Nakamura 2018; Lazzati et al. 2018; Margutti et al. 2017; Troja et al. 2017). Although the (50 – 300 keV)/(10 – 50 keV) hardness ratio is small ("soft"), the spectral peak energy is close to the lower end of the typical value in spite of the off-axis observation (but see Kisaka et al. (2017) for example). The rising X-ray and radio afterglow lightcurves as far as $\sim$ 100 days (Mooley et al. 2017; Ruan et al. 2017) are also difficult to explain with an off-axis afterglow model with a simple top-hat jet (or they may suggest a structured jet). GRB 170817A may belong to another population of gamma-ray transient phenomena other than the short GRB as proposed by Bromberg et al. (2017), Gottlieb et al. (2017), Kasliwal al. (2017), Murguia-Berthier et al. (2017), and Asano & To (2018). In such cases, the expected gamma-ray flux in the GeV range is not constrained by the previous short GRB observations.

The fluence of GRB 170817A in the keV-MeV energy band was observed to be $(1.4 \pm 0.3) \times 10^{-7}$ erg cm^{-2} (Abbott et al. 2017c). Had the same level of fluence been present in the GeV energy band, it could have be detected by GeV gamma-ray detectors in operation at that time. However, *Fermi*-LAT was entering the South Atlantic Anomaly and was not collecting data until about 10^3 seconds after GRB 170817A (Fermi-LAT collaboration 2017), and *AGILE* started observation after about 10^3 seconds (Verrecchia et al. 2017b). It was also out of the field-of-view of *CALET* as reported above. Thus unfortunately there is no limit in the GeV band around the trigger time of GW170817.

Regarding sGRB events in general, some events have been observed to emit high-energy ($>$ 100 MeV) gamma-rays (e.g., GRB 081024B, Abdo et al. (2010); and GRB 090510, Ackermann et al. (2010)). Their fluence in the high-energy band could be comparable to that in the hard X-ray band (Abdo et al. 2010). However, the fraction of GRBs showing high-energy emission observed to date is fairly low (Ackermann et al. 2013). This could be due to intrinsic properties associated with the gamma-ray emission mechanism, but another reason could be the limited field-of-view of GeV gamma-ray detectors ($2 \sim 3$ sr).

Figure 8 shows the sensitivity of *CALET*/CAL to obtain 1 event assuming an observation of 1, 10 and 100 s duration. The typical energy range of the on-axis gamma-ray emission from NS-NS mergers can be higher than that of the short GRB emission from GRB170817A. Although the effective area of *CALET*/CAL is smaller than that of *Fermi*-LAT, the fields-of-view of the two detectors are comparable. As the sensitivity of laser interferometers is expected to increase in coming years, the number of gamma-ray transients associated with GW events falling into the possible new population mentioned above will also increase. If their spectra extend to GeV energies, they could be easily detectable as shown in Figure 8. Thus *CALET*/CAL could contribute to constrain the GeV emission from a nearby NS-NS merger simultaneously with a GW signal in the near future. Monitoring the GeV sky with CALET, with its mission scheduled to continue for three more years, may complement the coverage by other missions and may help to study unexplored high-energy emission from future transient events.

We would like to thank the anonymous referee for comments and suggestions that materially improved the paper. We gratefully acknowledge JAXA's contributions for *CALET* development and operation on ISS. We express our sincere thanks to ASI and NASA for their support to the *CALET* project. This work is partially supported by JSPS Grant-in-Aid for Scientific Research (S) Number 26220708, JSPS Grant-in-Aid for Scientific Research (B) Number 17H02901, JSPS Grant-in-Aid for Scientific Research (C) Number 16K05382 and MEXT-Supported Program for the Strategic Research Foundation at Private Universities (2011-2015) S1101021 in Waseda University. This work is also supported in part by MEXT Grant-in-Aid for Scientific Research on Innovative Areas Number 24103002. US *CALET* work is supported by NASA under RTOP 14-APRA14-0075 (GSFC) and grants NNX16AC02G (WUStL), NNX16AB99G (LSU), and NNX11AE06G (Denver).

REFERENCES

Abbott, B. P. et al. 2016a, PhRvL, 116, 061102
Abbott, B. P. et al. 2016b, PhRvL, 116, 241103
Abbott, B. P. et al. 2016c, Phys. Rev. X, 6, 041015
Abbott, B. P. et al. 2017a, PhRvL,118, 221101
Abbott, B. P. et al. 2017b, PhRvL, 119, 141101
Abbott, B. P. et al. 2017c, PhRvL, 119, 161101
Abbott, B. P. et al. 2017d, ApJL, 848, L13
Abbott, B. P. et al. 2017e, ApJL, 848, L12

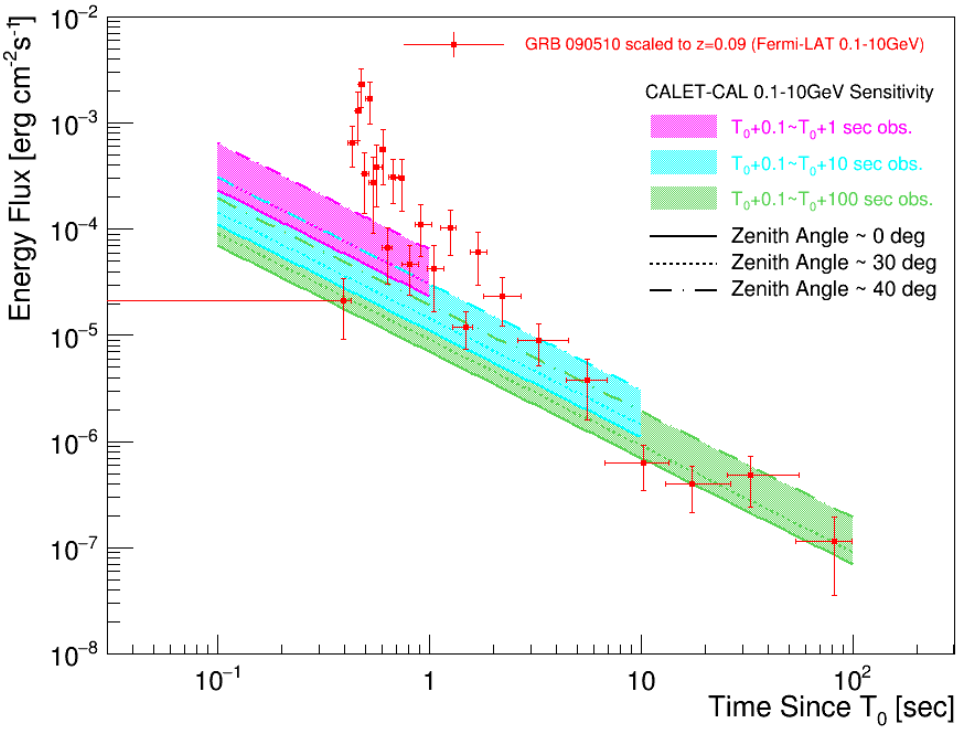

Figure 8. *CALET*/CAL sensitivity to obtain 1 event for a transient source assuming the energy spectrum proportional to $E^{-2}t^{-1}$, where E is the energy and t is the time after T_0, in the energy region 0.1 – 10 GeV. Despite the lack of sensitivity to sub-GeV gamma rays in the CAL, the 0.1 – 1 GeV band is included in this calculation of the limit to compare to the *Fermi*-LAT light curve since the energy flux is sensitive to the range over which it is integrated. Shaded areas show energy-flux sensitivities assuming observations of 1, 10 and 100 s duration for a source around the zenith, and dotted and dot-dashed lines show those for a source around 30° and 40° from zenith, respectively. Also shown by points are the observed light curve of GRB 090510 by *Fermi*-LAT , which is a short-hard GRB with an additional hard power-law component from 10 keV to GeV energies (Fermi-LAT collaboration 2017), scaled to $z = 0.09$, the nominal redshift of the first LIGO event GW150914 as calculated by Ackermann et al. (2016).

Abbott, B. P. et al. 2017f, ApJL, 851, L35

Abdo, A. A. et al. 2010, ApJ, 712, 558

Ackermann, M. et al. 2010, ApJ, 716, 1178

Ackermann, M. et al. 2013, ApJS, 209, 11

Ackermann, M. et al. 2016, ApJL, 823, L2

Acero, F. et al. 2016, ApJS, 223, 26

Adriani, O. et al. 2016, ApJL, 829, L20

Adriani, O. et al. 2017, PhRvL, 119, 181101

Akaike, Y. for the CALET Collaboration 2013, in Proc. 33rd ICRC (Rio de Janeiro, Brazil, 2013), 0726 (pp. 2162–2165).

Alexander, K. D., Berger, E., Fong, W., et al. 2017, ApJL, 848, L21

Asano, K., & To, S. 2018, ApJ, 852, 105

Asaoka, Y. et al. 2017, Astropart. Phys. 91, 1

Asaoka, Y. , Ozawa, S., Torii, S. et al. 2018, Astropart. Phys. 100, 29

Bromberg, O., Tchekhovskoy, A., Gottlieb, O., Nakar, E., & Piran, T. 2017, arXiv:1710.05897

Cannady, N. for the CALET Collaboration 2017, in Proc. 35th ICRC (Busan, Korea, 2017) (PoS (ICRC2017) 720)

Cannady, N. for the CALET Collaboration 2018, submitted for publication

de Mink, S. E. and King, A. 2017, ApJL, 839, L7

Eichler, D., Livio, M., Piran, T. & Schramm, D. N. 1989, Nature, 340, 126

Einstein, A., 1916, 1918, Sitzungsberichte der Königlich Preussischen Akademie der Wissenschaften Berlin, 1016, 688–696; *ibid.* 1918, 154–167.

Fermi-LAT collaboration 2017, arXiv:1710.05450

Fernández, R. & Metzger, B.D. 2016, Ann. Rev. Nucl. Part. Sci., 66, 23

Goodman, J. 1986, ApJ, 308, L47

Gottlieb, O., Nakar, E., Piran, T., & Hotokezaka, K. 2017, arXiv:1710.05896

Ioka, K., & Nakamura, T. 2018, Prog. Theor. Exp. Phys., 043E02

Kasliwal, M. M., Nakar, E., Singer, L. P., et al. 2017, Science, 358, 1559

Kisaka, S., Ioka, K., Kashiyama, K. & Nakamura, T. 2017, arXiv:1711.00243

Lazzati, D., Perna, R., Morsony, B. J., et al. 2018, PhRvL, 120, 241103
Margutti, R., Berger, E., Fong, W., et al. 2017, ApJL, 848, L20
Mochkovitch, R., Hernanz, J., Isern, J. & Martin, X. 1993, Nature, 361, 236
Mooley, K. P., Nakar, E., Hotokezaka, K., et al. 2017, Nature, 554, 207
Mori, M. for the CALET Collaboration 2013, in Proc. 33rd ICRC (Rio de Janeiro, Brazil, 2013), 0248 (pp. 1185–1188).
Murase, K. et al. 2018, ApJ, 854, 60
Murguia-Berthier, A., Ramirez-Ruiz, E., Kilpatrick, C. D., et al. 2017, ApJL, 848, L34
Narayan, R. Paczynsky, B. & Piran, T. 1992, ApJL, 395, L83
Omodei, N. et al. 2017, GCN, 21227
Pacyński, B. 1986, ApJ, 308, L43
Phinney, E. S. 2009, in New Worlds, New Horizons in Astronomy and Astrophysics (The National Academies Press) / arXiv:0903.0098
Pozanenko, A. et al. 2017, GCN, 21476
Racusin, J.L. et al. 2017, ApJ, 835, 82
Rosswog, S. 2015, Int. J. Mod. Phys., 24, 1530012
Ruan, J. J., Nynka, M., Haggard, D., Kalogera, V., & Evans, P. 2017, arXiv:1712.02809
Savchenko, V. et al. 2017, GCN, 21478
Torii, S. for the CALET Collaboration 2015, in Proc. 34th ICRC (Hague, Netherland, 2015) (PoS (ICRC2015) 581)
Troja, E., Piro, L., van Eerten, H., et al. 2017, Nature, 551, 71
Verrecchia, F. et al. 2017a, ApJL, 847, L20
Verrecchia, F. et al. 2017b, ApJL, 850, L27
Yamaoka, K. for the CALET Collaboration 2013, in Proc. 7th Huntsville Gamma-Ray Burst Symposium (Nashville, USA, 2013), paper 41/eConf Proceedings C1304143
Yamaoka, K. for the CALET Collaboration 2017, in Proc. 35th ICRC (Busan, Korea, 2017) (PoS (ICRC2017) 614)